DOI: 10.13009/EUCASS2019-644

Aerodynamic Design of a Reusable Booster Stage Flight Experiment

Clemens Merrem, Daniel Kiehn**, Viola Wartemann[+] and Thino Eggers[++]*

** German Aerospace Center (DLR), Institute of Aerodynamics and Flow Technology, Lilienthalplatz 7 38108 Braunschweig Germany, clemens.merrem@dlr.de*

*** German Aerospace Center (DLR), Institute of Flight Systems, Lilienthalplatz 7 38108 Braunschweig Germany, daniel.kiehn@dlr.de*

[+]German Aerospace Center (DLR), Institute of Aerodynamics and Flow Technology, Lilienthalplatz 7 38108 Braunschweig Germany, viola.wartemann@dlr.de

[++]German Aerospace Center (DLR), Institute of Aerodynamics and Flow Technology, Lilienthalplatz 7 38108 Braunschweig Germany, thino.eggers@dlr.de

Abstract

The German Aerospace Center is currently developing a flight experiment as a technology demonstrator for a reusable, horizontally landing booster stage, the Reusable Flight Experiment (ReFEx). The static and dynamic aerodynamic properties of the final shape of this 2.7 m long vehicle are presented in this paper. A two-staged VSB-30 sounding rocket transports ReFEx to an altitude of about 130 km. After the separation from the carrier rocket, an autonomous re-entry is performed with a maximum Mach number of approx. 5. The test flight of ReFEx is scheduled for 2022.

Abbreviations

6DoF	Six degrees of freedom
CFD	Computational Fluid Dynamics
ESA	European Space Agency
DLR	Deutsches Zentrum für Luft- und Raumfahrt (German Aerospace Center)
DoF	Degree(s) of freedom
EL	Euler
HEX	Hypersonic Flight Experiment
ISA	International Standard Atmosphere
LFBB	Liquid Fly-Back Booster
NS	Navier-Stokes
ReFEx	Reusability Flight Experiment
RLV-TD	Reusable Launch Vehicle Technology Demonstrator Programme
VTHL	Vertical take-off and horizontal landing
VTVL	Vertical Takeoff and Vertical Landing
WGS	World Geodetic System

Nomenclature

A	System matrix
a	Speed of sound
$C_{\{X,Y,Z\}}$	Force coefficients in x, y, and z direction
$C_{\{l,m,n\}}$	Moment coefficients around x, y, and z axis
H	Altitude
L	Reference length
Ma	Mach number
p, q, r	Roll rate, pitch rate, yaw rate
V	Airspeed

DOI: 10.13009/EUCASS2019-644

α	Angle of attack
β	Angle of sideslip
η	Symmetric canard deflection
δ	Vector of control surface deflections (canards and rudder)
ζ	Damping ratio
λ_i	i-th eigenvalue
ϕ	Roll angle
θ	Pitch angle
ω	Characteristic frequency
$\Omega^* = (p^*, q^*, r^*)^T$	Nondimensional rotational velocity vector

1. Introduction

A growing number of countries are seeking affordable ways to transport payload into orbits. One part of the effort to lower the prices is to design reusable rocket stages. Over the last decades, numerous experiments and ideas have been developed towards this idea.
Furthest in this segment is the US Company Space X with their Falcon Rocket. For their first rocket stage they pursue the strategy of vertical take-off and vertical landing (VTVL). They have successfully demonstrated this technology multiple times. The same principle is carried out by Blue Origin, also a US company.
The upside of VTVL is that no lift has to be generated through aerodynamic surfaces. Only relatively small fins are required to provide the stage with steering capabilities, resulting in comparably low structural mass. The landing capabilities are thus not strongly reliant on an atmosphere being present, which makes this technology applicable for a mars landing. Furthermore, the lower aerodynamic drag increases the aerodynamic efficiency during the ascent. As no significant lift can be generated, the deceleration of the stage has to be done through firing the engine in opposition to the flight direction. This requires additional fuel.
Taking advantage of the earth's atmosphere, another approach was investigated: Vertical take-off and horizontal landing (VTHL). The US Space Shuttle Orbiter (man graded spaceship) as well as the Russian Buran (prototype tested from lower heights) followed this principle by adding wings and fins to the configuration. Later, the US experimental X-37 followed. They were all designed for significantly higher velocities so a direct comparison is not possible. VTHL booster or first rocket stages are not in active use. Several case studies were conducted in search of a viable VTHL design. One was the USAF project Reusable booster System 2010 – 2012 having different US companies compete to design a reusable booster (Lockheed Martin won this competition). However, this was discontinued after two years. Another study was the liquid fly-back booster project from the German Aerospace Center (DLR) with the goal to design a reusable booster stage for the ESA's Ariane rocket from 1999 to 2004 [1]. The findings of this study are the starting point for the ReFEx project, in which a demonstrator will fly a realistic booster stage re-entry starting at 130 km and reaching maximum Mach numbers of approx. 5.
Comparable experiments are the Russian Baikal Booster which has a rotatable wing and a jet engine to return to the launch site airplane-like [2]. Its development is believed to have been completed in 2016. Reportedly, a prototype is being built [3]. Also there was the Hopper project of the ESA which resulted in the 7 m long Phoenix vehicle. It has short double delta wings and airplane-like landing gear. But the project was stopped after one successful drop test from a helicopter from around 2 km height in 2004 [4]. This experiment covered the landing phase. Another flown experimental vehicle is the Hypersonic Flight Experiment (HEX) from the Indian Reusable Launch Vehicle Technology Demonstrator Programme (RLV-TD) that was propelled to a height of 65 km at Ma = 5 in 2016. Reportedly, this 1 m diameter vehicle flew controlled for 770 s and ended its flight with a planned splashdown and was not recovered [5]. The midterm goal of the HEX vehicle, however, is to serve as a scramjet testing platform and therefore to withstand higher heat loads. Nevertheless, criteria such as navigation and control are quite comparable to ReFEx.
The project ReFEx allows progress on the combination of several systems and know-how areas needed to actually fly a reusable VTHL booster stage: Its starting point is outside of any noteworthy atmosphere, so the initial orientation is done via cold gas system. As the atmosphere's density increases, a short phase of overlapping control with the aerodynamic surfaces starts which then leads to aerodynamic forces taking over. Experience of this matter was already gained through the SHEFEX experiments [6].
Now the controllability is the main focus. ReFEx has three moveable surfaces: two all-moving canards and one classic flap in the tailing edge of the fin. The canards are relatively small, and their wake has a significant effect on the wings downstream. Therefore, close care to their aerodynamic behavior has to be taken.
Since the 14'' diameter ReFEx is already tightly packed with the necessary electronics, it is not equipped with landing gear. Therefore, the end of the experiment is reached when ReFEx passes through a target ellipsoid some

DOI: 10.13009/EUCASS2019-644

kilometers above ground. Nevertheless, touching ground as gently as possible will be tried to test the ground radar functionality within the system. As the entire experiment is over land, a recovery of ReFEx is planned although no parachute is installed.

1.1 Design Process

The starting point for ReFEx was the previously researched LFBB project from 2003 [7]. This predecessor was designed based on CFD simulations and fulfilled the static longitudinal stability criteria (Figure 1, left). It is a cylindrical fuselage shape with two canards (red), two wings, one body flap and a dihedral fin. For the former study, the canards and a body flap were actively used for steering.
Starting from this geometry, CFD simulations were carried out to determine the lateral stability characteristics. It soon became obvious that the vehicle was not laterally stable for high angles of attack. This is due to its fin being in the wake of the wings and the fuselage. To fix this, the two main options were either to move the fin out of the wake or to shift the center of gravity forwards. Moving the fin by tilting it to the side should have worked, however at this point the carrier rocket was chosen to be a VSB30, heavily limiting the aerodynamic design options. The following iterative design process consists of different loops, which are laid out here. More technical insight of the aerodynamic design process can be found in [7].

Figure 1: Geometry change over the course of the aerodynamic design. Left: Y8 (2003). Right: Y16 (2019).

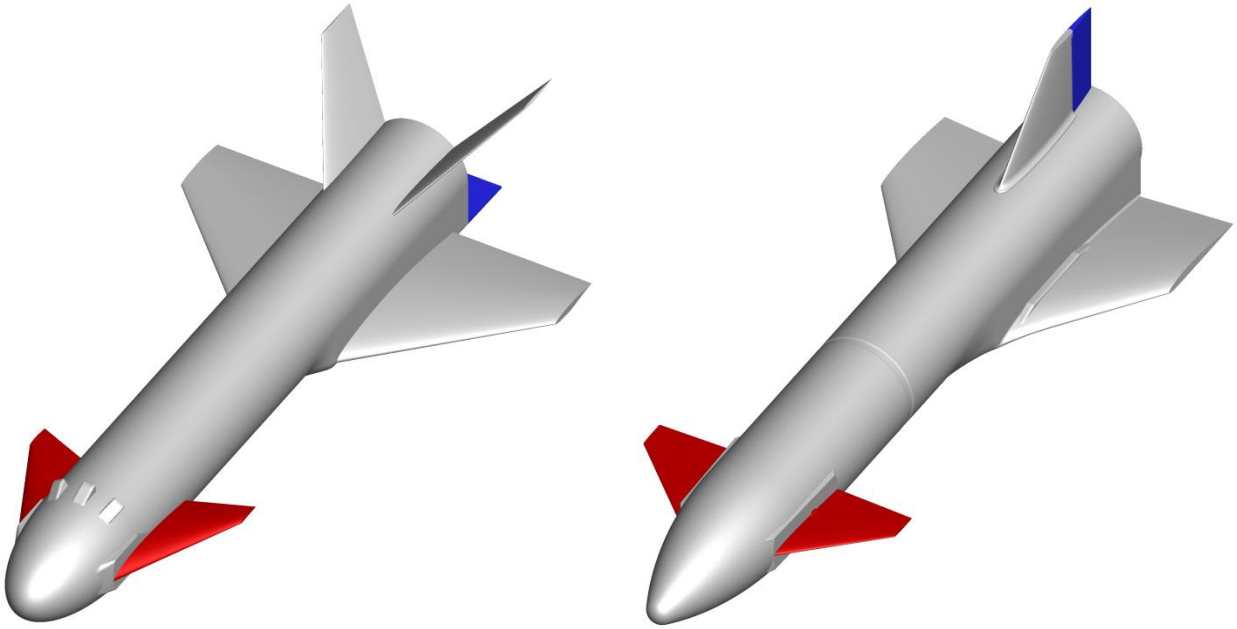

Each loop includes more departments, starting with only the aerodynamics department. This most inner loop had the most and fastest iterations. Often, several iterations within this loop were necessary to progress to the next step. This loop typically includes carrying our aerodynamic simulations and doing a check for aerodynamic static stability with the axis being mostly independent.
The next loop includes the department of flight systems and includes a more thorough investigation of stability with a flight dynamics model. Finishing this loop delivers a sufficiently stable and controllable flight configuration. For the final loop, other departments such as construction and payload design are involved to have an overall feasible vehicle.
It ultimately led to rather small changes compared to the original geometry (Figure 1, right). Starting from the front, the canards have the symmetrical NACA0008 profile. They are also mounted on a flat surface to reduce the gap to the fuselage when deflected. After the following cylindrical part, a wing box starts to ensure a smooth transition to the wings. The wings have an adapted Clark Y profile to have a flat lower surface. Lastly, for the geometry, the fin now is a single, vertical one, about the same size as the predecessor design. It has no special shape and simply is a smoothed double wedge. For steering purposes, the tailing part of the fin is a rudder.

DOI: 10.13009/EUCASS2019-644

1.2 Flight path overview

The flight of ReFEx is a controlled re-entry after being transported to a height of about 130 km with an apogee velocity of around 1 km/s. For the entire ascent the wing section of the vehicle is covered by a fairing to ensure symmetry. Outside of any notable atmosphere, the fairing is separated and the wings are expanded. Afterwards, a cold gas system rotates ReFEx into an aerodynamically stable orientation to ensure a smooth transition into the aerodynamically dominated flight phase. The first part of the following re-entry will be flown upside down at high (negative) angles of attack. During this phase, the maximum Mach number of approx. 5 is reached. At around Ma = 1.5, a 180° roll maneuver will be performed to reach the nominal orientation and to continue at moderate angles of attack (see Figure 2).
The controllable flight will be continued as long as possible, however the simulation results indicate declining controllability at Ma < 0.8. Therefore, the end of the experiment is defined at Ma = 0.8. The flight is planned to take place in Australia in 2022 (further details and explanations in [7] and [9]).

Figure 2: Flight envelope from static aerodynamic data with potential flight path.

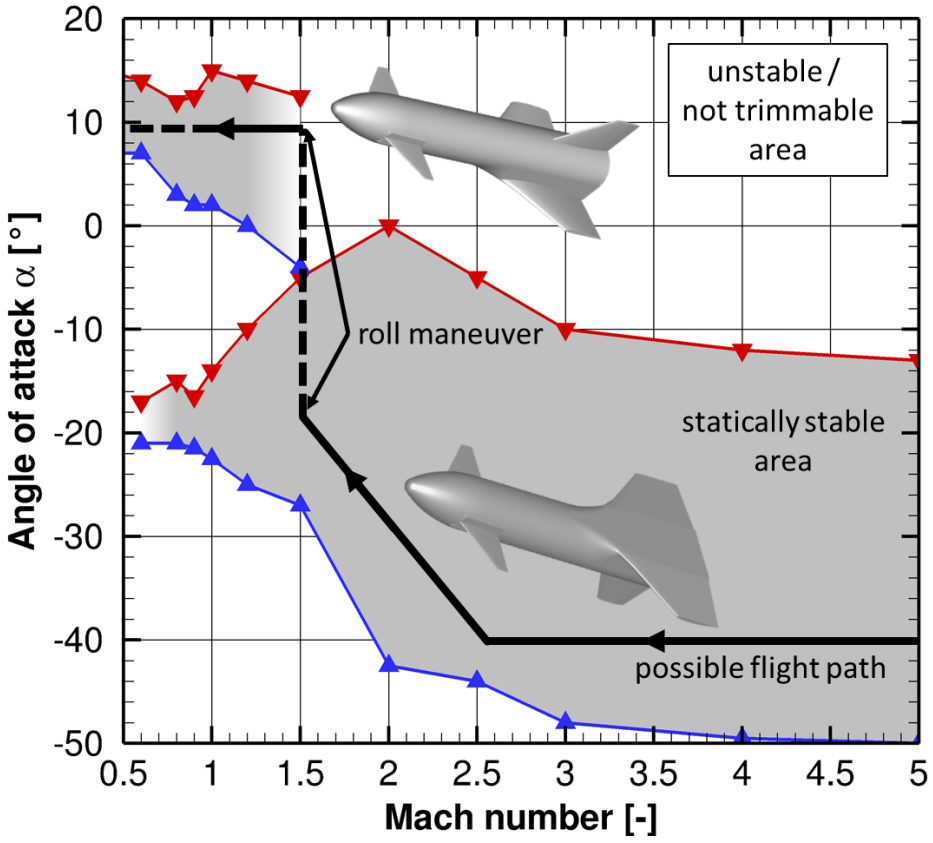

2. Tools and Methods

2.1 Simulations

For the aerodynamic characterization of ReFEx, a large number of CFD simulations were carried out with the DLR TAU Code (described in [10] [11] and [12]). It is a compressible flow solver. For this vehicle, unstructured and hybrid meshes with the mesh generator Centaur were used. The entire flight envelope was covered with data points for the aerodynamic coefficients. This required the variation of several parameters (see Table 1). However, not all of the arithmetical 12180 combinations (not including asymmetrical canard deflections) could be simulated within the given time frame. Subsequently, a reduction was required without losing critical information.
The first and most straightforward simplification was to split the dataset into a part of viscous Navier-Stokes (NS) simulations and inviscid Euler (EL) simulations. All aerodynamic coefficients except for the aerodynamic drag coefficient (and related coefficients) showed good agreement for Ma ≥ 2. The drag of the Euler simulations can be

DOI: 10.13009/EUCASS2019-644

corrected using the skin friction coefficient of a flat plate equivalent and the wetted surface of the vehicle. The required calculation time for one EL simulation is less than one tenth of a NS simulation.

Table 1: List of varied parameters of the aerodynamic data set.

Parameter	**Variation Range**	
	NS	**EL**
Mach number (Ma)	0.6 – 1.5, Δ = 0.1	2.0 – 6.0, Δ = 0.5
Angle of attack (α)	0° - 10°, Δ = 2.5	0° - 50°, Δ = 5.0
Canard deflection (η)	-15° - 15°, Δ = 5	-15° - 15°, Δ = 5
Sideslip angle (β)	0°, 1°, 5°	0°, 1°
Rudder deflection (ζ)	0°, 1°, 5°, 10°, 20°	0°, 1°, 5°, 10°, 20°
Number of variations	5250	6930

For both the NS and the EL areas, a mesh of simulation points was spanned around the planned trajectory, which was a result of the iterative design process (described briefly in chapter 1 and detailed in [8]). For these simulations, only Ma, α and symmetric η variations were considered. With this dataset, it was possible to acquire canard deflections for equilibrium of rotational accelerations over the entire Ma-α variating range. For all non-symmetric parameters (side-slip angle β, asymmetric canard deflections and the rudder deflection) this was used as reference to deviate around. The entirety of all simulations thus far described was the static aerodynamic data base which will be used to describe the vehicle. By these measures, the new count of necessary simulations was reduced to 5220 (2250 NS + 2970 EL), including asymmetrical canard deflections of ±1° and ±5°. Additional simulations might be necessary for the roll maneuver at Ma = 1.5.

2.2 Stability analysis

2.2.1 Flight dynamics model

The flight dynamics model used for the stability analysis of ReFEx is implemented in MATLAB/Simulink™. It incorporates the nonlinear six-degrees-of-freedom (6DoF) equations of motion in a quaternion-based implementation, a WGS-84 geodetic model [13], and the international standard atmosphere (ISA) model [14]. The aerodynamic coefficients required to calculate aerodynamic forces and moments are obtained via interpolation on lookup tables. Each force coefficient $C_{\{X,Y,Z\}}$ and moment coefficient $C_{\{l,m,n\}}$ is modelled as a sum of static and dynamic contributions, i.e.

$$C_{(.)} = \underbrace{C_{(.),static}}_{f(Ma,\alpha,\beta,\delta)} + \underbrace{C_{(.),dyn}}_{g(Ma,\alpha,\eta,\Omega^*)} \quad \textbf{(1)}$$

where $(.)$ is a generic placeholder for any force $\{X,Y,Z\}$ or moment $\{l,m,n\}$, Ma is the Mach number, α is the angle of attack, β is the angle of sideslip, δ is the set of individual deflections of the canards and rudder (with η being the symmetric canard deflection), and Ω^* is the nondimensional rotational velocity vector, defined by

$$\Omega^* = \begin{pmatrix} p^* \\ q^* \\ r^* \end{pmatrix} = \frac{L}{V}\begin{pmatrix} p \\ q \\ r \end{pmatrix} = \frac{L}{a \cdot Ma}\begin{pmatrix} p \\ q \\ r \end{pmatrix} \quad \textbf{(2)}$$

where L represents the reference length, V is the (true) airspeed and a is the speed of sound.
Assuming perfect x-z-symmetry of the vehicle, the contributions of the dynamic derivatives to the moment coefficients are obtained via:

$$\begin{pmatrix} C_l \\ C_m \\ C_n \end{pmatrix}_{dyn} = \begin{pmatrix} C_{lp} & 0 & C_{lr} \\ 0 & C_{mq} & 0 \\ C_{np} & 0 & C_{nr} \end{pmatrix}\begin{pmatrix} p^* \\ q^* \\ r^* \end{pmatrix} \quad \textbf{(3)}$$

DOI: 10.13009/EUCASS2019-644

Note that for a constant altitude (hence constant speed of sound a) and constant dynamic derivatives, the absolute contribution of the dynamic terms to the total coefficients $C_{(.)}$ due to a given rotational rate decreases with increasing Mach numbers [15].

2.2.2 Trimming and linearization

First, the model is trimmed at the flight point (which is mainly characterized by the altitude H, the Mach number and the angle of attack) using the canards and rudder to achieve an equilibrium of rotational accelerations, i.e. $\dot{p} = \dot{q} = \dot{r} = 0$. Translational accelerations have to be accepted as they cannot be compensated directly due to the absence of an engine or additional control surfaces. The sideslip angle β is set to zero, representing the nominal flight condition of the vehicle.
The model is then linearized numerically around the trim point using central differences to obtain the system matrix A and its eigenvalues λ_i, which are used for the stability analysis. Given a symmetrical flight condition (i.e. $\beta = p = q = r = 0$ and $\phi = 0$ or $\phi = 180°$), the system matrix A can be split up into A_{lon} describing the longitudinal motion and A_{lat} describing the lateral motion [16]. In the presented case, the longitudinal motion comprises the states $(H, V, \alpha, \theta, q)^T$, typically including the phugoid and short period oscillations and the height mode. The lateral motion, on the other hand, comprises the states $(\phi, \beta, p, r)^T$ and typically includes the Dutch roll motion as well as the spiral divergence and the roll subsidence modes. Note that the aforementioned typical modes may be observable only in certain flight regimes (e.g. the height mode becomes insignificant in subsonic flight [17]) and can differ substantially from the characteristic motions of conventional aircraft. The complex eigenvalues λ_i yield the damping ratio ζ_i and the characteristic angular frequency ω_i of the corresponding motion via: [18]

$$\omega_i = \|\lambda_i\| = \sqrt{\mathrm{Re}(\lambda_i)^2 + \mathrm{Im}(\lambda_i)^2} \tag{4}$$

$$\zeta_i = \frac{-\mathrm{Re}(\lambda_i)}{\omega_i} \tag{5}$$

To evaluate the stability of the vehicle at a certain flight point, the eigenvalues of longitudinal motion and lateral motion are analyzed separately, and for each the maximum occurring real part is stored. For the final evaluation, only the maximum real part $\mathrm{Re}_{\max}$ of both regimes of motion (longitudinal *and* lateral) is considered:

$$\mathrm{Re}_{\max} = \max\left(\mathrm{Re}(\lambda_{\mathrm{i,lon}}), \mathrm{Re}(\lambda_{\mathrm{i,lat}})\right) \tag{6}$$

Using the maximum real part, the damping ratio and the frequency of the least stable motion can be covered with a single criterion which is in turn used to find a suitable trajectory or flight corridor. All flight points are categorized into separate groups based on their maximum real parts $\mathrm{Re}_{\max}$ to find a Ma/α/altitude corridor in which the vehicle is sufficiently stable and controllable according to Table 2:

Table 2: Stability categories based on the maximum real part.

Maximum real part Re_{max}	**Category**	**Flight point accepted**	**Color in Figure 5 and Figure 9**
$\mathrm{Re}_{max} \leq 0$	Natural or neutral stability	Yes	Green
$0 < \mathrm{Re}_{max} \leq 0.05$	Minor instability	Yes	Yellow
$0.05 < \mathrm{Re}_{max} \leq 0.01$	Major instability	Yes	Orange
$\mathrm{Re}_{max} > 0.1$	Critical instability	No	Red
N/A	Insufficient control authority	No	Gray

The application of this categorization is explained in detail in [19].

DOI: 10.13009/EUCASS2019-644

2.3 Aerodynamic dynamic derivatives

After concluding that a rolling maneuver is necessary to fulfill the trajectory requirements, an impact of dynamic aerodynamic effects became likely. Also controlling the energy dissipation to follow the target trajectory is done via banking maneuvers. Therefore, an investigation of these effects was conducted.
The dynamic aerodynamic damping is a consequence of the vehicles movement. This vehicles movement changes the flow field, thus changing the aerodynamic coefficients dependent on the movement. A positive damping is referred to as an induced moment counteracting the movement whereas a negative damping amplifies it. As described in Section 2.2, a linearized approach to characterize the stability was used. As dynamic contribution, only the dependencies on the rotation rates were taken into account.
The approach used on this matter was to look at the effects of the coefficient derivatives resulting from rotation around the body fixed axis. In the DLR Tau Code, a fixed rotational rate around any axis can be set in a static simulation. The effect of this is a curved flow field around the chosen axis passing through a chosen point. An example with a rotation around the body-fixed y-axis is shown in Figure 3, left. The intensity of the curving of the flow field depends on the chosen rotation rate and the vehicles velocity.
The information gained through this process is the difference in rotational acceleration from a flight condition of the case with and without the investigated dynamic damping coefficients.

Figure 3: Curved flow field of static pitch rate simulation and derivative behavior at different rotation rates.

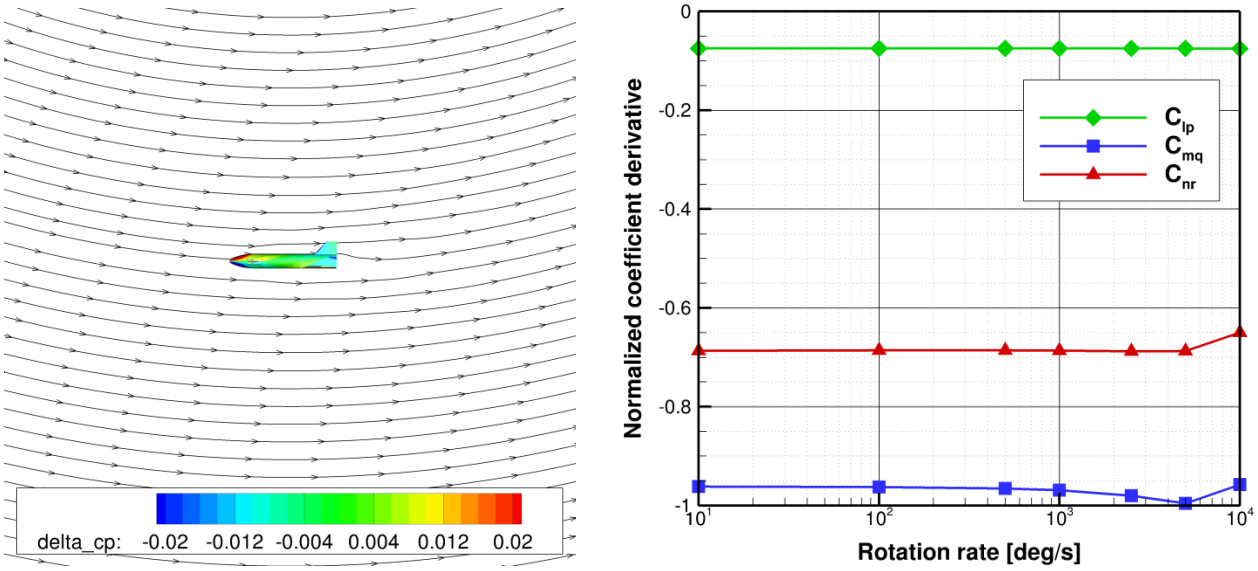

The difference in the surface pressure coefficient in comparison to the case without any rotational rates was calculated (see Figure 4). Red areas mark additionally induced pressure coefficient areas, whereas blue areas mark the opposite. This change in pressure distribution leads to a change of the aerodynamic coefficient. The rate of the coefficient changes are correlated to the aerodynamic damping. The linearization of these derivatives only should be valid if they behave linearly within the range of rotation rates of interest, which for ReFEx are estimated not to exceed 500 deg/s. This behavior is displayed in Figure 3, right, where linearity up to 10000 deg/s is shown. Therefore, it is valid to simulate the dataset with just one rotational rate per axis.

DOI: 10.13009/EUCASS2019-644

Figure 4: Rotation rate induced differential pressure coefficient distribution with q = 100 deg/s and Ma = 4.

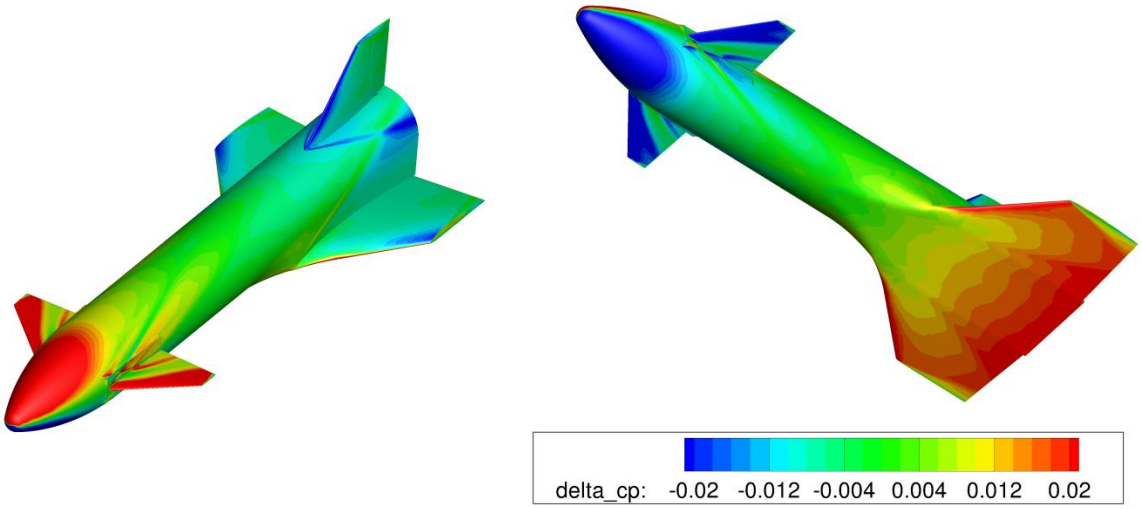

3. Results and Evaluation

3.1 Static Aerodynamic Properties of ReFEx

The main goal of the aerodynamic investigation was to determine the range of trimmable (where equilibrium of moments can be achieved), aerodynamically stable and controllable Ma-α-altitude combinations to find a suitable flight corridor. This is achieved through the procedure described in section 2.2.2 (see [19] for details). The first step was to analyze only static stability, i.e. dynamic derivatives were not included in the aerodynamic model. The resulting flight envelope is shown in Figure 5 for a fixed altitude of H = 2 km. The main effect of varying the altitude for a given Mach number is that it changes the dynamic pressure depending on the ambient pressure, and it changes the absolute airspeed due to the varying ambient temperature and hence varying speed of sound. The value of 2 km was chosen because it represents the approximate altitude range where the vehicle is foreseen to be exposed to subsonic Mach numbers, which was found to be a critical flight regime. Note that when dynamic derivatives are disregarded, there is no trimmable and sufficiently stable flight corridor at Mach 0.4, i.e. the vehicle could not maintain controlled flight if the aerodynamic model was accurate and the acceptable value for $\mathrm{Re}_{\mathrm{max}}$ of 0.1 is realistic.

Figure 5: Flight envelope for H = 2 km, disregarding dynamic derivatives.

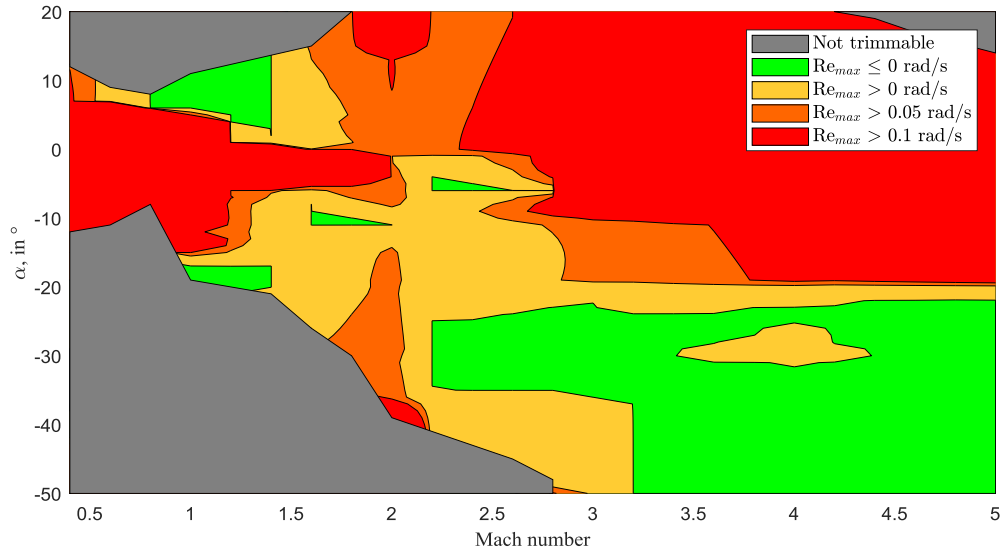

DOI: 10.13009/EUCASS2019-644

3.2 Results of the Aerodynamic Simulations with Static Rotation Rates

The influence of the rotation rates was characterized with two datasets of Ma-α fields, one NS simulation set and one EL set. All Ma-α combinations were simulated with rotation rates around the body fixed x-, y- and z-axis. The derivative was determined with the respective coefficient from a simulation without rotation rates. The main rotational derivatives are C_{mq}, C_{lp} and C_{nr} (see Figure 6 to Figure 8). All other rotation rate derivatives (e.g. C_{lr} and C_{np}) were significantly smaller and therefore, their effect should be negligible. The absolute value of the derivatives is an indication of the effect it will have on the vehicle. Negative values represent damping of movement, whereas positive values accelerate movement. Every pair of NS and EL plots has the same scaling to enable better comparison.

The first pair (Figure 6) shows the most influential derivative C_{mq}. The flow condition is the same as the above described example with an induced pitch rate. Moving though the Ma-α range starting at the highest Mach number at an angle of attack around -40° yields a C_{mq} value of -2.6. While lowering the Mach number from this point but maintaining the angle of attack, this value only changes slightly over the Mach number down to two. If the movement critical for stability is influenced by this derivative, for the flight path at α = -40°, a constant change of stability would be expected. In the NS area, the derivative changes heavily with the Mach number. At α = 8°, values between -2.6 and -3.6 would occur, yielding changing damping characteristics.

The yawing moment derivative C_{nr} has slightly smaller numbers (Figure 7). Looking at a flight path in the EL set at α = -40° gives values from -1.5 to -1.8. A slight damping increase from Mach 6 to 2. The NS set however has an almost constant value around -1.2 over the entire Ma-α field.

Lastly, the roll damping derivative C_{lp} (see Figure 8) has values which are smaller than the pitch damping derivative C_{mq} (see Figure 6). This is due to the relatively small wings yielding a smaller lever for the respective forces compared to the lever through the length of the vehicle. The respective damping is smaller; however the acting moments are smaller as well. In the lower Mach number area, the roll damping is even lower at -0.15.

Figure 6: Normalized pitching moment derivative C_{mq} for ReFEx. Left: NS data set. Right: EL data set.

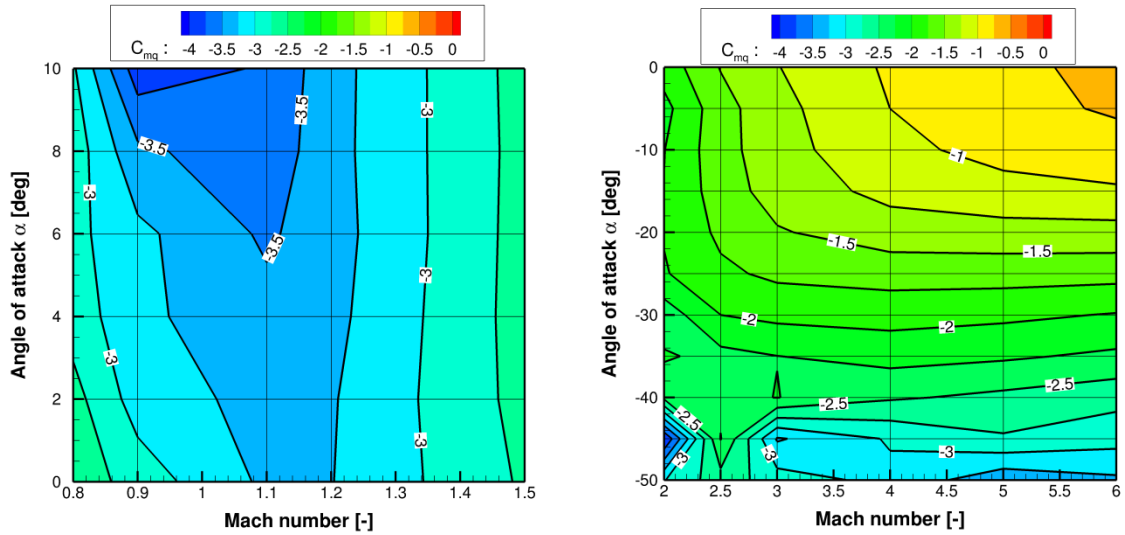

DOI: 10.13009/EUCASS2019-644

Figure 7: Normalized yawing moment derivative C_{nr} for ReFEx. Left: NS data set. Right: EL data set.

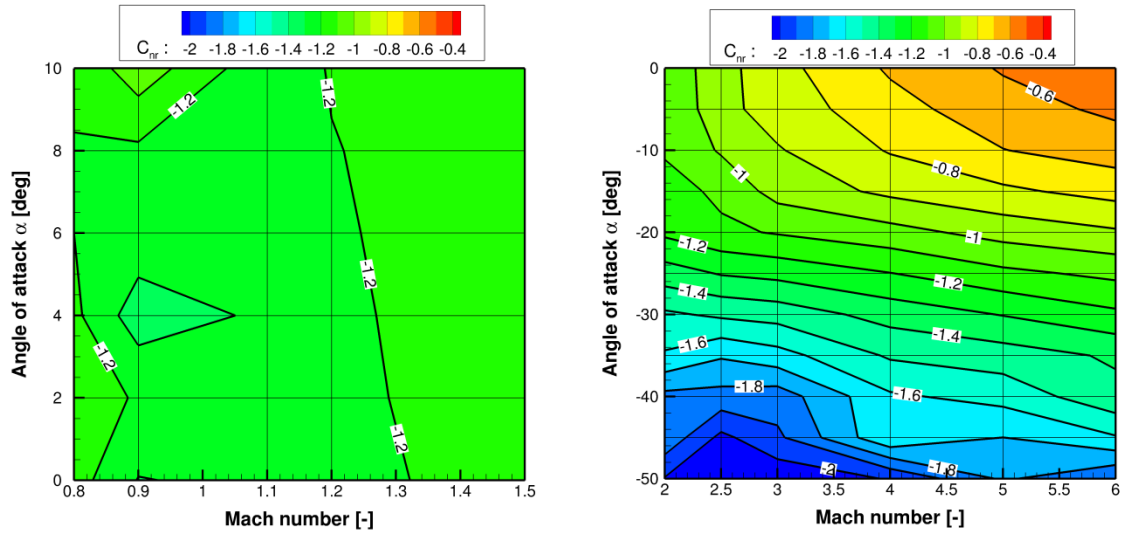

Figure 8: Normalized rolling moment derivative C_{lp} for ReFEx. Left: NS data set. Right: EL data set.

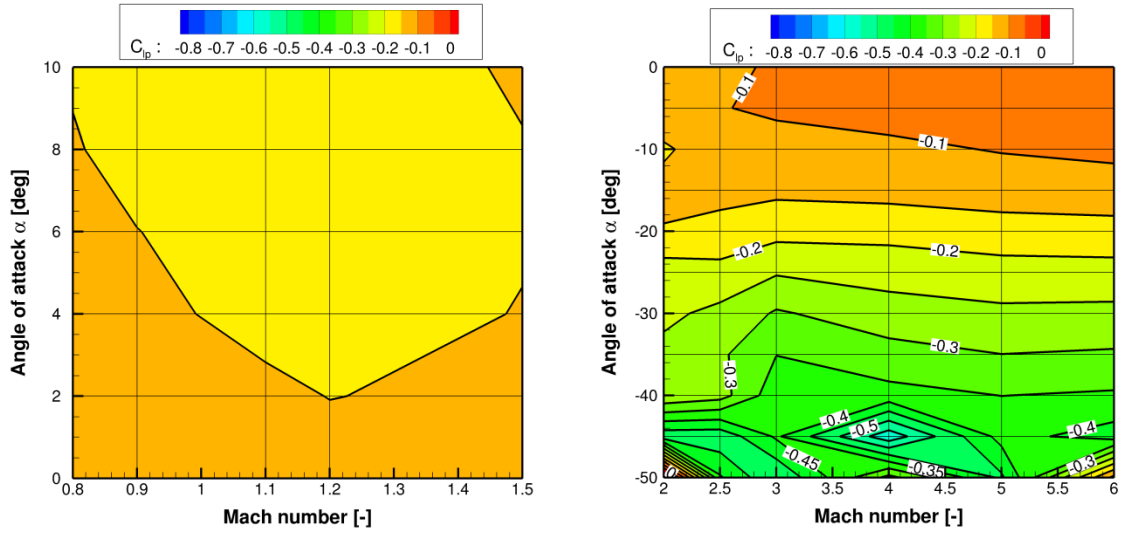

Even though the absolute value of the derivative is an indicator of the damping, no information on the type of movement critical for the stability is provided. Only the correlation of the damping with the movement yields the stability improvement through the damping derivatives.

3.3 Evaluation of the impact of dynamic derivatives

To evaluate the impact of the dynamic derivatives on the flight envelope of the vehicle, the stability analysis explained in section 2.2.2 is conducted, but dynamic derivatives are taken into account as well. The resulting 2-dimensional flight envelope for a fixed altitude of H = 2 km is shown in Figure 9.

DOI: 10.13009/EUCASS2019-644

Figure 9: Flight envelope for H = 2 km including dynamic derivatives, regions of interest are marked in black.

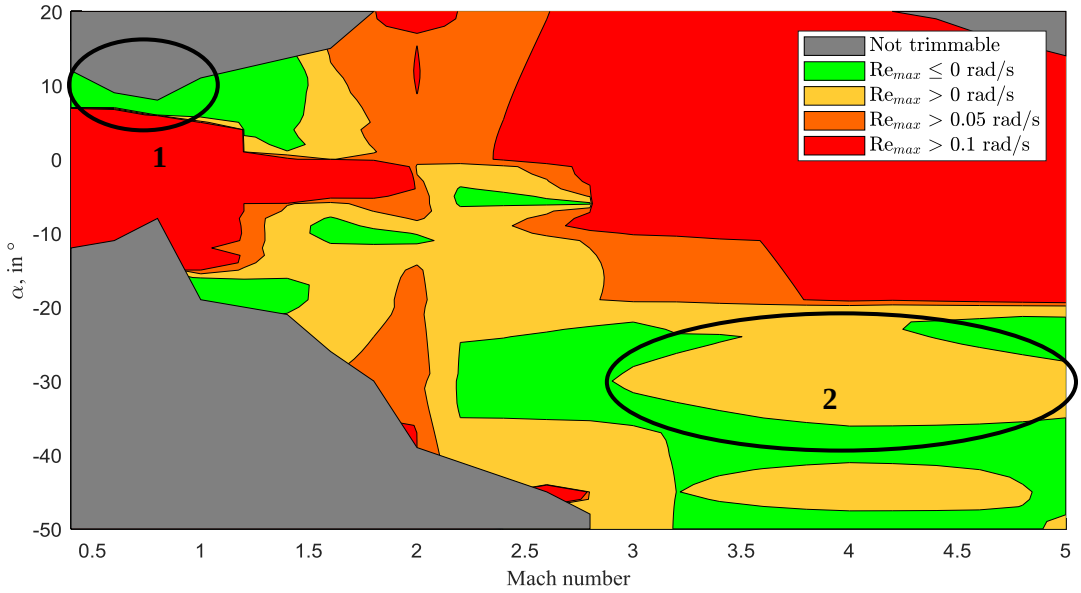

The main effects of the dynamic derivatives on the stability and the flight envelope can be observed by comparing the regions 1 and 2 in Figure 9 with the corresponding regions in Figure 5. Two regions can be identified where the effects of the dynamic derivatives appear to be most significant: first, subsonic to low transonic flight ($0.4 \leq \text{Ma} \leq 0.8$) at relatively low angles of attack (approx. $\alpha = 8°$), and second, supersonic flight ($3 \leq \text{Ma} \leq 5$) at high negative angles of attack. Both of the aforementioned regions of interest will now be discussed in detail.

3.3.1 Region 1: subsonic flight, moderate angles of attack

Considering the dynamic damping, region 1 now shows a small naturally stable corridor at low Mach numbers (Ma < 0.8) around $\alpha = 8°$. The eigenvalues of the longitudinal and lateral motion for $\alpha = 8°$ and $0.4 \leq \text{Ma} \leq 0.8$ are visualized in Figure 10 and Figure 11. It can be seen that the short period motion is stabilized by the dynamic derivatives as was expected. The damping ratio, while still quite low, has increased and the angular frequency has increased very slightly. However, if only the maximum real parts are considered as mentioned in section 2.2.2, the phugoid or height modes are considered as more critical in both cases due to their real parts being close to zero. Since these modes are primarily energy based, they are almost unaffected by dynamic derivatives, as can be seen in Figure 10.
The lateral motion however shows a different picture: the Dutch roll, which was unstable for approx. $\text{Ma} \geq 0.6$ and represented the most critical characteristic motion, is completely stabilized taking dynamic derivatives into account. As a consequence, the longitudinal and the lateral motion are stable if dynamic derivatives are considered; hence there is now a suitable (green) corridor at low Mach numbers if dynamic damping is included (Figure 9) which does not occur when it is excluded (Figure 5).

DOI: 10.13009/EUCASS2019-644

Figure 10: Eigenvalues of longitudinal motion, α = 8°, 0.4 ≤ M a ≤ 0.8, ΔMa = 0.025.

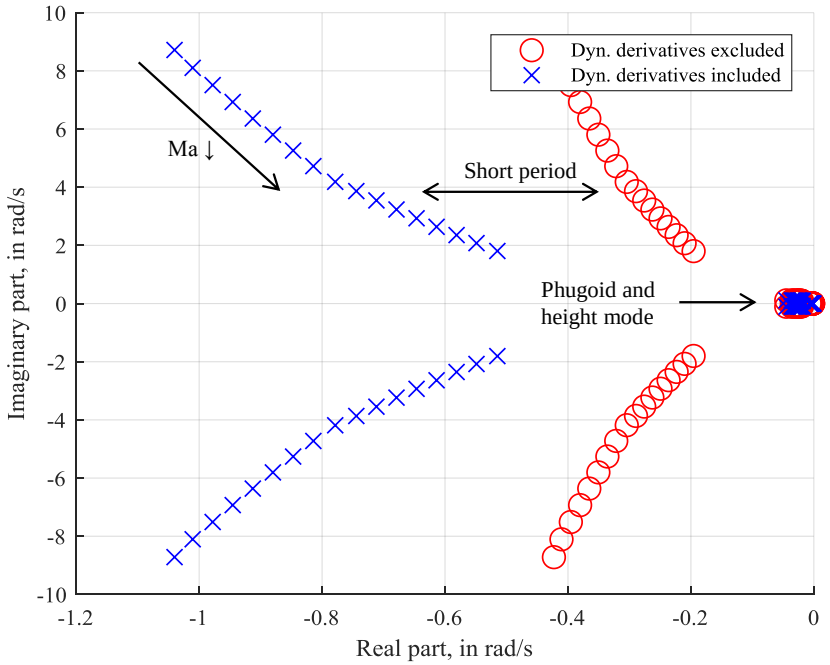

Figure 11: Eigenvalues of lateral motion, α = 8°, 0.4 ≤ M a ≤ 0.8, ΔMa = 0.025.

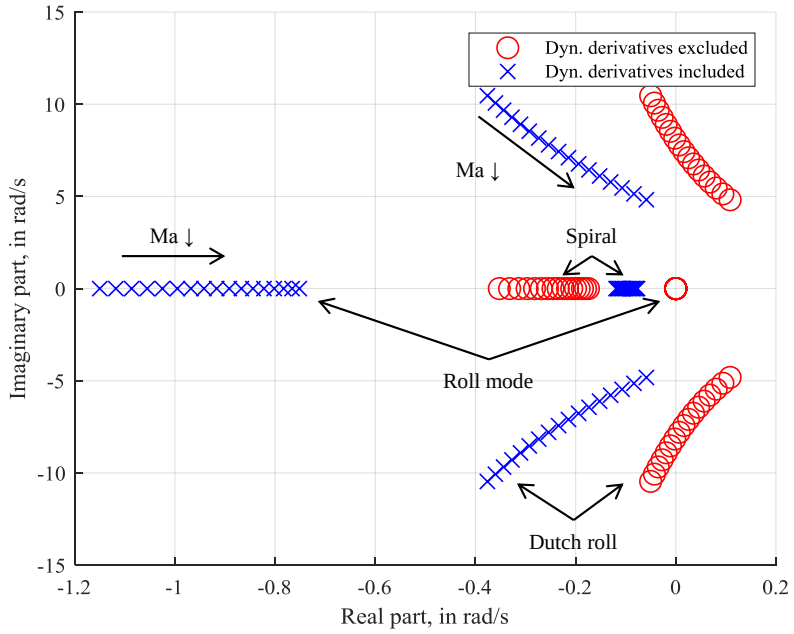

3.3.2 Region 2: supersonic flight at high negative angles of attack

At higher Mach numbers (3 ≤ Ma ≤ 5) and high negative angles of attack, the stability appears to slightly decrease if dynamic derivatives are taken into account. Looking at the eigenvalues of the longitudinal motion for α = -30° (Figure 12), it can be seen that the damping ratio and the angular frequency of the short period motion slightly increase. The phugoid and height modes are again nearly unaffected.

DOI: 10.13009/EUCASS2019-644

The lateral motion (see Figure 13) on the other hand shows a slight decrease of overall stability in the sense of the maximum real part: while the Dutch roll and the roll mode are further stabilized, the spiral get slightly destabilized: there is a very small shift of the real parts into the positive direction (see Figure 14). The shift is marginal, but due to the chosen thresholds used for stability categorization the change appears in the envelope plot (Figure 9).

Figure 12: Eigenvalues of longitudinal motion, α = -30°, 3 ≤ Ma ≤ 5, ΔMa = 0.1.

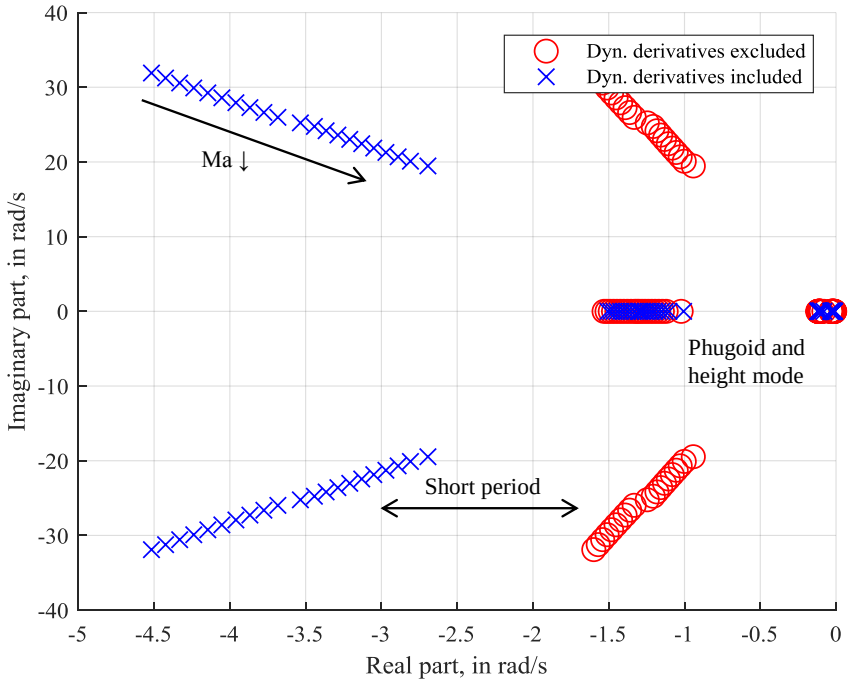

Figure 13: Eigenvalues of lateral motion, α = -30°, 3 ≤ Ma ≤ 5, ΔMa = 0.1.

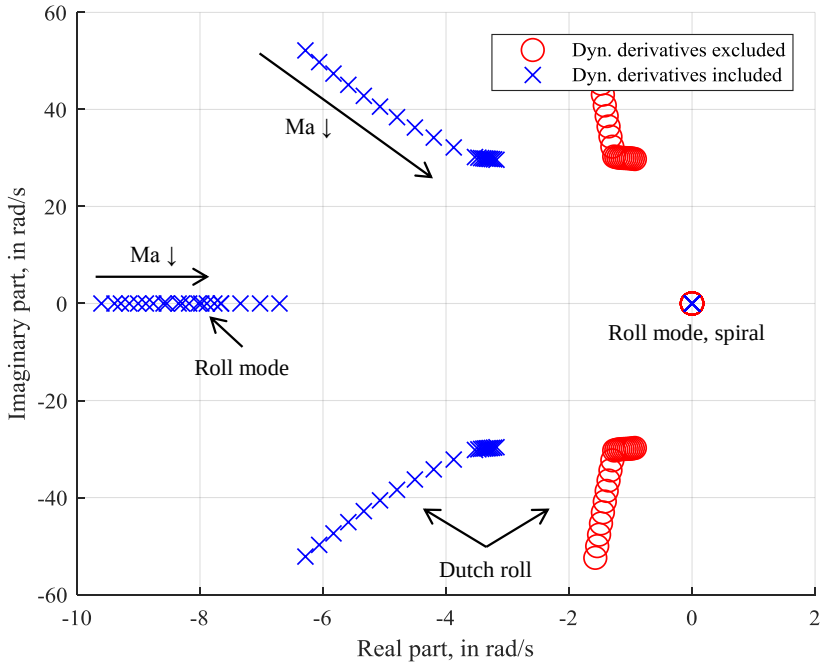

DOI: 10.13009/EUCASS2019-644

Figure 14: Real parts of the spiral mode vs. Mach number, α = -30°, 3 ≤ Ma ≤ 5, ΔMa = 0.1.

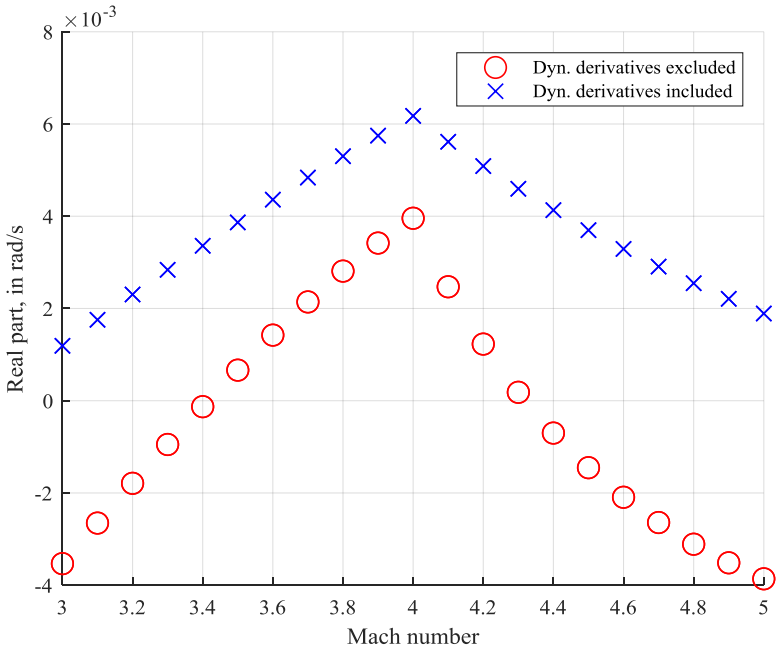

4. Conclusion

The aerodynamic design of the flight experiment ReFEx was continued to the point of a configuration freeze. A stability analysis yielded a feasible flight path regarding stability and controllability. Since the preliminary design studies, several iterative design loops with involved disciplines have been completed, increasing the confidence in the presented geometry.

The presented data gives a characterization of the dynamic aerodynamic stability of ReFEx over the re-entry envelope. The focal point lies on the question whether the flyable envelope is enlarged through the inclusion of rotation rate induced moment derivatives. On this matter, two areas with different behaviour were identified. First, in the subsonic region at low angles of attack, the stability improvement was significant, especially at very low Mach numbers. This is thought to be due to the fact the rotational rates become more significant relative to the airspeed of the vehicle, as discussed in section 2.2.2. The effect of the dynamic derivatives greatly increases the flight envelope in this region. In fact, there is no suitable flight corridor if they are disregarded. In supersonic speeds approx. between Mach 3 and 5, the stability is decreased very slightly. This effect, however, is so small that it is considered negligible, especially considering that the unstable motion is the spiral and even many commercial aircraft inhere an unstable spiral to maintain some degree of lateral maneuverability [16].

Overall, for a vehicle like ReFEx, the inclusion of rotation rate derivatives at Mach numbers lower than 2.0 yields improvements that justify the additional simulation workload. Especially, if the flyable corridor is narrow or ends at some Mach number, it has the greatest potential benefit. At high Mach numbers, the steering margins should be large enough, so the minor changes should not have an impact and therefore, an investigation seems not to be necessary.

4.1 Future investigations

At this point, the aerodynamic investigation of ReFEx only lacks two potentially important aspects. The first is the roll behaviour. Due to the canard configuration, the canard's deflection significantly changes the flow around the downstream wing. For pitching purposes, this is great because stronger canard deflection lead to less lift at the wing. This enhances the pitch capability. However because of the small wing to canard size ratio, this may lead to a rudder reversal and needs to be investigated thoroughly.

The second point is the behavior due to thermal elongation. Because the trajectory areas with high heat load are flown upside down, the upper hull area will heat up. The consequence is a bending of the vehicle and therefore, a change of the relative position of wings to canards. In combination with the roll movement characteristics, this may lead to problems and needs to be investigated. Further, thermal analysis will be conducted to quantify the thermal loads due to aerodynamics. This is critical to ensure both the structural stability and the functionality of all internal electronics. In the end, a trade-off between thermal bending and additional mass/change of materials has to be done.

DOI: 10.13009/EUCASS2019-644

References

[1] Sippel, M., Manfletti, C., Burkhardt, H., & Eggers, T. (2003). Technical development perspective of reusable booster stages. In *12th AIAA International Space Planes and Hypersonic Systems and Technologies* (p. 7057).

[2] A. Medvedev, Yu. Trufanof, E. Pashkov, E. Motorniy, Potentialities of multi-functional application for "Baikal" 1-stage reusable Booster, IAF 2001, Toulouse, IAF 01-V.4.09.

[3] Cherberco, I.: «Роскосмос» готовится к созданию многоразовой ракетыа (engl.: "Roscosmos" is preparing to create a reusable rocket), Izvestia Newspaper website article. (2016) https://iz.ru/news/619896, accessed: June 2019.

[4] Gockel, W., Kyr, P., Janovsky, R., & Roenneke, A. (2005). Reusable RLV Demonstrator Vehicles-Phoenix Flight Test Results and Perspectives. *Space Technology*, *25*(1), 1-14.

[5] Yadav, S., Jayakumar, M., Nizin, A., Kesavabrahmaji, K., & Mohan, N. S. (2017). Final Phase Flight Performance and Touchdown Time Assessment of TDV in RLV-TD HEX-01 Mission. *Journal of The Institution of Engineers (India): Series C*, *98*(6), 679-688. Eggers, Th.: Aerodynamic Behaviour of a Liquid Fly-back Booster in Transonic Cruise Flight. AIAA Paper 2003-3422 (2003).

[6] Bierig A., Lorenz S., Spangenberg H. (2013). Development of the Aerodynamic Control System for the Hypersonic Flight Experiment SHEFEX II. Deutscher Luft- und Raumfahrtkongress (DLRK) 2013.

[7] Eggers, Th.: Aerodynamic Behaviour of a Liquid Fly-back Booster in Transonic Cruise Flight. AIAA Paper 2003-3422 (2003).

[8] Merrem C., Wartemann V., Eggers Th.: Preliminary Aerodynamic Design of a Reusable Booster Flight Experiment. HiSST Paper 2018-857 (2018).

[9] Rickmers, P.: ReFEx: Reusability Flight Experiment. A Flight Experiment to Demonstrate Controlled Aerodynamic Flight from Hypersonic to Subsonic Velocities with a Winged RLV. EUCASS 2017-644 (2017). https://doi.org/10.13009/EUCASS2017-644.

[10] Mack, A., Hannemann, V.: Validation of the Unstructured DLR TAU-Code for Hypersonic Flows. AIAA Paper 2002-3111 (2002).

[11] Schwamborn, D., Gerhold, T., and Heinrich, R., "The DLR TAU-Code: Recent Applications in Research and Industry," Proceedings of the European Conference on Computational Fluid Dynamics, edited by Wesseling, P., Oñate, E., and Périaux, J., Delft Univ. of Technology, Delft, The Netherlands (2006).

[12] Gerhold, T., Galle, M., Friedrich, O., and Evans, J., "Calculation of Complex Three Dimensional Configurations Employing the DLR-Tau Code," 35th Aerospace Sciences Meeting and Exhibit, AIAA Paper 1997-0167 (1997).

[13] US Department of Defense, 2000. World Geodetic System 1984. National Imagery and Mapping Agency, USA.

[14] International Organization for Standardization (ISO) 2533:1975.

[15] Hankey, W. 1988. Re-Entry Aerodynamics. AIAA Education Series, Dayton, Ohio.

[16] Brockhaus, R., Alles, W., Luckner, L. 2011. Flugregelung, 3. Auflage. Springer Verlag, Berlin.

[17] Sachs, G. 1993. Novel Stability and Control Problms of Aerospace Planes. IFAC 12th Triennial World Congress, Sydney, Australia.

[18] Etkin, B., and Reid, L. 1996. Dynamics of Flight: Stability and Control, 3rd Edition. John Wiley & Sons, Toronto, Canada.

[19] Schwarz, R., Wenzel, A., Kiehn, D., Trigo, G., Razgus, B., Solari, M., Bestard Körner, M., Dumke, M., Reigenborn, M., Seelbinder, D., Theil, S., Pfau, D., Sommer, J., Braun, B., Markgraf, M. : Overview of Flight Guidance, Navigation, and Control for the DLR Reusability Flight Experiment (ReFEx). EUCASS 2019, Madrid, Spain.